Winding numbers of nodal points in Fe-based superconductors

Dmitry V. Chichinadze and Andrey V. Chubukov

Winding numbers of nodal points in Fe-based superconductors

Dmitry V. Chichinadze and Andrey V Chubukov[1]

[1]*School of Physics and Astronomy, University of Minnesota, Minneapolis, MN 55455, USA*

We analyze the nodal points in multi-orbital Fe-based superconductors from a topological perspective. We consider the s^{+-} gap structure with accidental nodes, and the d-wave gap with nodes along the symmetry directions. In both cases, the nodal points can be moved by varying an external parameter, e.g., a degree of inter-pocket pairing. Eventually, the nodes merge and annihilate via a Lifshitz-type transition. We discuss the Lifshitz transition in Fe-based superconductors from a topological point of view. We show, both analytically and numerically, that the merging nodal points have winding numbers of opposite sign. This is consistent with the general reasoning that the total winding number is a conserved quantity in the Lifshitz transition.

I. INTRODUCTION

The research on correlated electron systems over the last decade have shown tremendous developments in two seemingly different areas. One area, generally termed as "topology in condensed matter", focuses on topological description of quantum materials, with emphasis on specific invariants which characterize a particular quantum state of matter, and change only when a system undergoes a transition from one quantum state to the other. The research in this field started in the early 80's [1–3], but rapidly accelerated over the last decade and led to qualitative new understanding of the properties of existing materials and to discoveries of numerous new materials exhibiting fundamentally novel properties [4–7]. Another area is high-temperature superconductivity. The research in this field started after the discovery of SC in the cuprates [8–10] and acquired a new dimension with the invent of Fe-based superconductors (FeSCs) with multiple relevant orbitals and, as a consequence, multiple Fermi pockets of hole and electron-type [11].

Some FeSCs exhibit superconducting properties consistent with the full gap, while the others show behavior consistent with gap zeros on some of the Fermi surfaces [12–14]. A number of theories have been put forward about s-wave superconductivity in FeSCs with orbitally-induced gap anisotropy. When the anisotropy is strong enough, an s-wave gap can have nodes on some of the pockets [15–19]. Because the gap nodes are accidental, they can appear or disappear via a Lifshitz-type transition [20] under the change of external parameters like doping or pressure [13, 21]. In special cases (which we discuss below), the transition from a nodal state to a state with a full gap is more involved, with additional nodal points appearing near a transition and then annihilating the existing nodes [22]. Another set of theories for FeSCs analyzed possible d-wave superconductivity, particularly in systems where only hole or only electron pockets are present. In a one-band system a d-wave superconductor has symmetry protected gap nodes on the Fermi surface. In multi-band materials, like FeSCs, these nodes can also be manipulated by, e.g., varying the strength of the inter-band pairing [19, 23]. In the presence of such terms, the nodal points of the fermionic dispersion in a d-wave superconductor shift from the original Fermi surfaces to the area between the pockets, come closer to each other and eventually annihilate and disappear, leaving a d-wave superconductor with a full gap [19, 23].

In this paper we discuss Lifshitz transitions in FeSCs from a topological viewpoint. We argue that, while the symmetry of a superconducting state ($d-$wave or $s-$wave) does not change upon the apperance/disappearance of the zeros in the fermionic dispersion, the topological properties of a system do change because each nodal point is characterized by a particular winding number, which remains invariant as long as a nodal point exists, but vanishes once it disappears.

We study two models of FeSCs, one with an s-wave gap symmetry and accidental gap nodes, and another with a d-wave gap and nodes along particular symmetry directions. In both models, the nodes can be manipulated by changing one or more model parameters. As a result, a system may undergo a Lifshitz transition in which the nodal points merge and disappear. We show, both analytically and numerically, that the merging nodal points have opposite sign winding numbers. We also show that when a pair of nodal points is spontaneously generated by changing an external parameter, the winding numbers of the two emerging nodes are opposite. This is consistent with the general reasoning that the total winding number is a conserved quantity in the Lifshitz transition. Such a result may sound intuitively obvious, but we emphasize that in each model the total number of nodal points is equal to eight, and it is not a'priori guaranteed that the neighboring nodal points (the ones which will eventually merge) have opposite winding numbers. This has to be verified in explicit calculations.

The merging and annihilation of nodal points has been studied in Dirac and Weyl semi-metals, which undergo a transition into an insulator under a variation of certain system parameters [24]. Several authors have shown that in a semi-metal-to-insulator transition, the merging nodal points have opposite winding numbers [25, 26]. However, the analysis of the winding numbers of the nodal points in in s-wave and d-wave superconductors has not been presented in the literature, as far as we know.

The structure of the paper is as follows. In Sec. II we

introduce the Berry curvature $B_{\vec{k}}$ and express the winding number as a particular 2D integral of $B_{\vec{k}}$. In Sec. III we consider a model of an s-wave superconductor which undergoes a Lifshitz transition upon varying one or more system parameters [22], and compute the winding numbers of the nodal points near the transition. In Sec. IV we consider a two-orbital/two band model of a d-wave superconductor, which also undergoes a Lifshitz transition [19] when the pairs of nodal points along a symmetry direction merge and annihilate. We again compute winding numbers of these nodal points. Finally, we make several concluding remarks in Sec. V.

II. THE BERRY PHASE AND THE WINDING NUMBER

The topological properties of a system of interacting electrons in two dimensions (2D) are generally defined in terms of the Berry phase [3, 27–29]. This phase reflects a non-trivial topological structure of the wave function in the Hilbert space in the presence of topological defects, such as nodal points. The Berry phase γ, is the phase which a wave function $\left| n(\vec{R}) \right\rangle$ acquires when a system moves along a close path C around a topological defect in the space specified by the set of parameters $\vec{R}$ [29, 30]:

$$\gamma = -\oint_C d\vec{R} \cdot A_{\vec{R}} = -\int_{\mathcal{S}} d\vec{S} \cdot B_{\vec{R}},$$

Here $\mathcal{S}$ represents a closed surface in the parameter space, enclosed by the contour C, $A_{\vec{R}} = -\text{Im} \left\langle n(\vec{R}) \right| \nabla_{\vec{R}} \left| n(\vec{R}) \right\rangle$, and $B_{\vec{R}} = \nabla_{\vec{R}} \times A_{\vec{R}}$. The quantities $A_{\vec{R}}$ and $B_{\vec{R}}$ are called the Berry connection and the Berry curvature. In our case the parameter set is specified by momentum $\mathbf{k}$. The winding number Q is defined as the "normalized" Berry phase [27–30]

$$Q = -\frac{1}{2\pi} \oint_C d\vec{k} \cdot A_{\vec{k}} = -\frac{1}{2\pi} \int dk_x dk_y \left(\frac{\partial A_{k_y}}{\partial k_x} - \frac{\partial A_{k_x}}{\partial k_y} \right). \quad (1)$$

In 2D systems this topological invariant represents an obstruction to the Stokes theorem and detects the presence of the nodal points [29, 31]

A standard recipe to obtain Q for systems with nodal points is to expand the dispersion in the vicinity of the node. A generic Hamiltonian near a nodal point can be cast into the form

$$H = -(k_i - k_i^0) A_{ij} \sigma_j, \quad (2)$$

where k_i^0 – coordinates of the nodal point and σ_j are the Pauli matrices. For the effective Hamiltonian describing the low-energy band of two-dimensional superconducting system the matrix A_{ij} is a 2×2 diagonal matrix which plays a role of "metric tensor". Then the sign of the determinant of

this matrix reflects orientation of the basis (i.e. is it right-handed or left-handed) thus leading to the expression for the winding number $Q = -sign[\det(A)]$, that can also be understood through geometrical argument presented below.

Here we provide a simple geometrical argument to compare the winding numbers for different nodal points. Namely, suppose that there are two nodal points 1 and 2. One can compute winding numbers $Q(1)$ and $Q(2)$ by integrating along two different contours, each surrounding only one nodal point. Both contours should have the *same* direction of bypass. Alternatively, one can transform the coordinates, separately for region 1 and region 2, and bring the nodes to the same point in space. The integration contours then become the same, modulo the direction of the bypass. The winding numbers $Q(1)$ and $Q(2)$ then are equal if the bypass directions in new basis are the same, or have opposite signs if the bypass directions in new basis are opposite.

In the next two sections we compute Q for two models of FeSCs. We first compute Q analytically and then verify the results numerically, using the computational method which has been proposed in Ref. [32].

III. AN s-WAVE SUPERCONDUCTOR WITH ACCIDENTAL NODES

A. The model

We consider a 2D model of an FeSC with hole pockets centered at $\Gamma = (0, 0)$ and electron pockets centered at $(0, \pi)$ and $(\pi, 0)$ in 1Fe Brillouin zone (BZ). We assume that the dominant interaction is in the s-wave (A_{1g}) channel, and the system develops an s^{+-} superconductivity with π phase difference between the gaps on hole and electron pockets. The gaps on Γ-centered hole pockets are C_4 symmetric, with $\cos 4n\theta_h$ variation along the hole pockets. The electron pockets are centered at non-C_4-symmetric points, and the gap variation along the electron pockets has additional $\pm \cos(4m + 2)\theta_e$ components (with θ_e counted from the same axis on both electron pockets). We assume, following earlier works, that the $\cos 2\theta_e$ variation is the strongest one, and it gives rise to accidental nodes on the electron pockets. The gap on hole pockets has no nodes, and we will not include hole pockets into our consideration.

The position of the accidental nodes can be manipulated by including the hybridization between the two electron pockets [18, 22]. The hybridization is caused by pnictogen/chalcogen atoms, which are located above and below an Fe plane, in "up-down" order. As a result, the actual unit cell is bigger and contains 2 Fe atoms. One can still work in a 1Fe unit cell, but there the hybridization gives rise to terms in the Hamiltonian, in which incoming and outgoing momenta differ by (π, π). In a superconductor, there are two types of such terms – one describes the hopping between the electron pockets, another describes a creation or anni-

hilation of Cooper pairs made of fermions from different electron pockets. Both terms affect the position of the gap nodes. For definiteness, here we consider the effects due to additional pairing terms induced by the hybridization.

The Hamiltonian of the model is

$$H = H_0 + H_\Delta + H_\beta \tag{3}$$

where

$$H_0 = \sum_k \xi_k^c c_{k\alpha}^\dagger c_{k\alpha} + \xi_k^d d_{k\alpha}^\dagger d_{k\alpha} \tag{4}$$

is the kinetic energy of fermions near the two electron pockets,

$$H_\Delta = \frac{1}{2} \sum_k \left[\Delta_c \, c_{k\alpha}^\dagger c_{-k\beta}^\dagger + \Delta_d \, d_{k+Q\alpha}^\dagger d_{-k-Q\beta}^\dagger \right] i\sigma_{\alpha\beta}^y, \tag{5}$$

is the pairing term with angle-dependent gap functions $\Delta_c = \Delta(1 - y_e)$, $\Delta_d = \Delta(1 + y_e)$, where $y_e = \alpha \cos 2\theta_e$, and α is a parameter, which depends on the orbital composition of electron pockets. When $\alpha > 1$, Δ_c and Δ_d have accidental nodes. Finally,

$$H_\beta = \frac{1}{2} \sum_k \beta \left[c_{k\alpha}^\dagger d_{-k-Q\beta}^\dagger + d_{k+Q\alpha}^\dagger c_{-k\beta}^\dagger \right] i\sigma_{\alpha\beta}^y \tag{6}$$

is the additional pairing term, induced by the hybridization, in which the total momentum of the pair equals to (π, π). Without the loss of generality we set β to be positive. We will see that by varying the strength of β one can move the positions of the accidental nodes.

It is instructive to consider separately the special case, when the electron pockets can be approximated as circular, and a generic case, when they are elliptical. For both cases we assume that $\alpha > 1$, i.e., in the absence of hybridization the gap functions Δ_c and Δ_d have accidental nodes.

1. Circular pockets

For circular electron pockets $\xi_k^c = \xi_k^d = \xi_k$. The Hamiltonian (3) can be straightforwardly diagonalized by Bogoliubov transformation to [22]

$$H = E_0 + \sum_{k,\alpha} E_k^+ e_{k\alpha}^\dagger e_{k\alpha} + E_k^- f_{k\alpha}^\dagger f_{k\alpha} \tag{7}$$

where

$$\left(E_k^\pm \right) = \left[\xi_k^2 + \left(\Delta \pm \sqrt{\Delta^2 y_k^2 + \beta^2} \right)^2 \right]^{1/2} \tag{8}$$

The dispersion E^+ is obviously nodeless, but E^- has zeros at

$$\cos(2\theta_e) = \pm \frac{\sqrt{\Delta^2 - \beta^2}}{\alpha\Delta}. \tag{9}$$
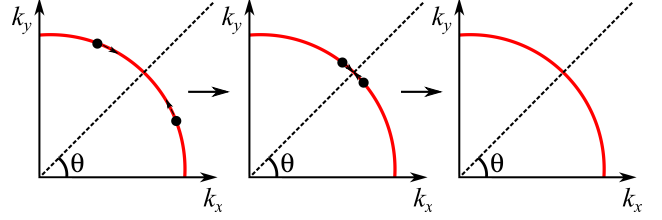

FIG. 1. The location of the nodal points on one of the FS of hybridized circular electron pockets. Red line – the first quadrant of the FS, black dots – the nodal points. The nodes move towards BZ diagonals (in 1Fe zone) with increasing the strength of the hybridization parameter β. The neighboring nodal points merge and disappear at $\beta_{\text{crit}} = \Delta$.

At $\beta < \beta_{\text{crit}} = \Delta$ there are 8 nodal points, two in each of the four quadrants. At the critical value $\beta = \beta_{\text{crit}}$ the pairs of nodal points merge along the BZ diagonals. At $\beta > \beta_{\text{crit}}$, the nodes disappear (see Fig. 1).
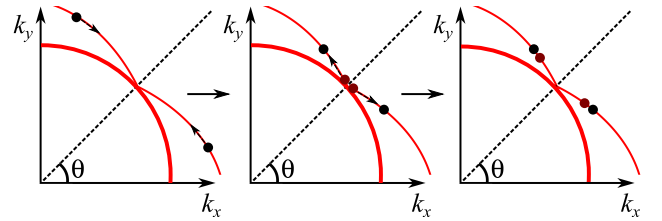
2. Elliptical pockets

FIG. 2. The location of the nodal points on one of the FS of hybridized elliptical electron pockets, for large enough degree of ellipticity. Thick red line – the first quadrant of the FS, thin red line – the locus of location of the nodal points, black dots – the original nodal points. As the hybridization parameter β increases, nodal points move towards the BZ diagonal, but don't reach it. Instead, at $\beta = \Delta$, a new pair of nodal points (brown dots) appears along BZ diagonal, and at larger β move towards the existing nodes. The old and the new nodal points merge and disappear at $\beta = \beta_{\text{crit}} > \Delta$.

For elliptical pockets the dispersions are

$$\xi_k^c = \frac{k_x^2}{2m_1} + \frac{k_y^2}{2m_2} - \mu, \quad \xi_k^d = \frac{k_x^2}{2m_2} + \frac{k_y^2}{2m_1} - \mu, \tag{10}$$

expanding near the Fermi surface we obtain [22, 33]

$$\xi_k^{c,d} = \xi_k \pm \delta \cos(2\theta_k),$$

$$\delta \approx k_F^2 \frac{m_2 - m_1}{4m_1 m_2}, \quad \xi_k = k^2/2m^* - \mu, \quad m^* = 2m_1 m_2/(m_1 + m_2) \tag{11}$$

Diagonalizing the Hamiltonian we again obtain two bands

with the dispersion $(E^{\pm}) = \left(A_k \pm \sqrt{B_k}\right)^{1/2}$, where

$$A_k = \frac{1}{2}\left[(\xi_k^c)^2 + (\xi_k^d)^2 + 2\Delta^2(1 + y_k^2) + 2\beta^2\right],$$

$$B_k = \frac{1}{4}\left[\left((\xi_k^d)^2 - (\xi_k^c)^2 + 4\Delta^2 y_k\right)^2 + 4|\beta|^2\left((\xi_k^c - \xi_k^d)^2 + 4\Delta^2\right)\right]. \tag{12}$$

Using Eqs. (11) we can rewrite (E^-) as

$$(E^-) = \left[\xi_k^2 + \Delta^2 + \beta^2 + \cos^2(2\theta)\left(\delta^2 + \Delta^2\alpha^2\right) - \right.$$

$$\left. 2\sqrt{\cos^2(2\theta)\left(\Delta^2\alpha - \xi\delta_k\right)^2 + |\beta|^2\left(\delta^2\cos^2(2\theta) + \Delta^2\right)}\right]^{1/2}. \tag{13}$$

In distinction to circular pockets, nodal points are now located not on the original Fermi surface, but at

$$\xi = \frac{\delta^2 - \alpha^2\Delta^2 \pm \sqrt{(\alpha^2\Delta^2 + \delta^2)^2 - 4\alpha^2\beta^2\delta^2}}{2|\alpha|\delta},$$

$$\cos^2(2\theta) = \frac{\delta^2 - \alpha^2\Delta^2 \mp \sqrt{(\alpha^2\Delta^2 + \delta^2)^2 - 4\alpha^2\beta^2\delta^2}}{2\alpha^2\delta^2}. \tag{14}$$

A straightforward analysis shows [22] that the evolution of the nodal points with increasing β depends on the interplay between the ellipticity parameter δ and $\alpha\Delta$. When $\delta < \alpha\Delta$, pairs of nodes in each quadrant merge and disappear at $\beta = \Delta$ on the diagonals of the BZ, like in the case of circular pockets. When $\delta > \alpha\Delta$, nodal points don't reach diagonals when β reaches Δ. At this β, a new pair on nodes appears along each diagonal (see Fig. 2). As β continues increasing, the new nodal points move towards the existing nodes. The new and old nodes merge and disappear at the critical

$$\beta_{\mathrm{crit}} = \frac{\alpha^2\Delta^2 + \delta^2}{2|\alpha|\delta} > \Delta. \tag{15}$$

B. The winding number

1. Circular pockets

To obtain the winding numbers for the nodal points we expand E_k^- in Eq. (8) near each of 8 nodal points. Because of C_4 symmetry, we only consider the first quadrant $\theta \in [0, \pi/2]$. The dispersion (8) near a nodal point has the Dirac form

$$E_k^{\mathrm{Dirac}} = \sqrt{\left(\frac{d\xi}{dk}(k - k')\right)^2 + \left(\frac{2\Delta^2\alpha^2\sin(2\theta)\cos(2\theta)}{\sqrt{\Delta^2\alpha^2\cos^2(2\theta) + \beta^2}}(\theta - \theta')\right)^2}, \tag{16}$$

where $k' = k_F$ and θ' are the coordinates of $E_k^- = 0$. The corresponding Dirac Hamiltonian can be obtained using the
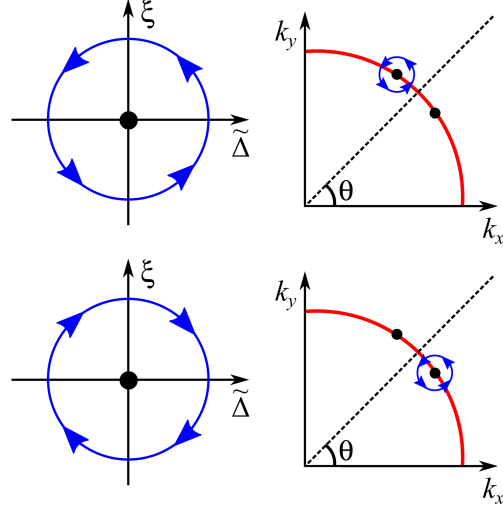

FIG. 3. Winding around each of the two nodal points shown in the right panel. Both points are mapped to the origin of the coordinates by transforming to the new basis with variables $(\xi, \tilde{\Delta})$ instead of (k_x, k_y) (left panel). Different winding numbers for the two nodes on the right panel and due to different directions of bypass on the left panel.

Pauli matrices

$$H^{\mathrm{Dirac}} = \frac{d\xi}{dk}(k - k') \cdot \sigma_3 + \frac{\Delta^2\alpha^2\sin(4\theta)}{\sqrt{\Delta^2\alpha^2\cos^2(2\theta) + \beta^2}}(\theta - \theta') \cdot \sigma_1, \tag{17}$$

or, in the explicit matrix form,

$$H^{\mathrm{Dirac}} = \begin{pmatrix} \frac{d\xi}{dk}(k - k') & \frac{\Delta^2\alpha^2\sin(4\theta)}{\sqrt{\Delta^2\alpha^2\cos^2(2\theta)+\beta^2}}(\theta - \theta') \\ \frac{\Delta^2\alpha^2\sin(4\theta)}{\sqrt{\Delta^2\alpha^2\cos^2(2\theta)+\beta^2}}(\theta - \theta') & -\frac{d\xi}{dk}(k - k') \end{pmatrix}. \tag{18}$$

We associate θ with the first nodal direction and k with the third one, and rewrite Dirac Hamiltonian H^{Dirac} in the form of Eq. (2) with A_{ij} ($i, j = 1, 3$)

$$A = \begin{pmatrix} \frac{\Delta^2\alpha^2\sin(4\theta)}{\sqrt{\Delta^2\alpha^2\cos^2(2\theta)+\beta^2}} & 0 \\ 0 & \frac{d\xi}{dk} \end{pmatrix}. \tag{19}$$

The sign of the det A depends only on sign of $\sin(4\theta)$, which is positive at $\theta < \pi/4$ and negative at $\theta > \pi/4$. Nodal points are located on the opposite sides of $\theta = \pi/4$, hence their winding numbers are opposite: -1 and +1.

We can obtain the same result by introducing the effective pairing Hamiltonian for fermions with E_k^- in the form

$$H_{eff} = \begin{pmatrix} \xi & \tilde{\Delta} \\ \tilde{\Delta} & -\xi \end{pmatrix} \tag{20}$$

with $\tilde{\Delta} = \Delta - \sqrt{\Delta^2 y_k^2 + \beta^2}$, and treating $(\xi, \tilde{\Delta})$ as new effective coordinates. The transformation from (k_x, k_y) to $(\xi, \tilde{\Delta})$

is multi-valued: all 8 solutions for $E_k^- = 0$ are now mapped to the origin in $(\xi, \tilde{\Delta})$-plane. Then the contour C in Eq. (1) is the same for all nodal points, and the signs of the winding numbers depend only on the bypass direction of C for a given node (which is a topological invariant). Because $\tilde{\Delta}$ depends on $\cos 2\theta$, we have different direction of bypass for each pair of nodal points in a given quadrant (see Fig. 3). Indeed, consider the nodal point located between $\theta = 0$ and $\pi/2$. Let's choose the counterclockwise bypass along the closed contour in the (k_x, k_y)-plane. The bypass starts at $\xi = 0$, $\theta > \theta_{\rm sol}$ and goes to the point $\xi < 0$, $\theta = \theta_{\rm sol}$, where $\theta_{\rm sol}$ is the solution for $\tilde{\Delta} = 0$. One can easily verify that this corresponds to clockwise bypass direction in the $(\xi, \tilde{\Delta})$-plane. Using the same strategy, one can then verify that the same bypass in the (k_x, k_y)-plane for another nodal point (the one with larger $\theta_{\rm sol}$) corresponds to counterclockwise direction in the $(\xi, \tilde{\Delta})$-plane. This obviously gives the opposite sign of the winding number.

2. Elliptical pockets

We now extend the analysis to elliptical pockets. We expand the Hamiltonian of Eq. (3) in Taylor series in the vicinity of each nodal point and obtain the Dirac Hamiltonian in the form

$$H = \begin{pmatrix} \frac{dE^-}{dk^2}\frac{dk^2}{dk}(k-k') & \frac{dE^-}{d\theta}(\theta-\theta') \\ \frac{dE^-}{d\theta}(\theta-\theta') & -\frac{dE^-}{dk^2}\frac{dk^2}{dk}(k-k') \end{pmatrix}. \quad (21)$$

Associating $\theta - \theta'$ and $k - k'$ with the directions $i = 1$ and $i = 3$, respectively, we obtain the matrix A in Eq. (2), as

$$A = \begin{pmatrix} \frac{dE^-}{d\theta} & 0 \\ 0 & \frac{dE^-}{dk^2}\frac{dk^2}{dk} \end{pmatrix}, \quad (22)$$

where

$$\frac{dE^-}{dk^2} = \frac{X - Y\cos^2(2\theta)}{\sqrt{D}} \\ \frac{dE^-}{d\theta} = \frac{Z\sin(4\theta)}{\sqrt{D}} \quad (23)$$

and

$$D = \beta^2 + \Delta^2 + \xi_k^2 + \left(\delta^2 + \alpha^2\Delta^2\right)\cos^2(2\theta) \\ -2\sqrt{\beta^2\Delta^2 + (\beta^2\delta^2 + (\alpha\Delta^2 - \delta\xi_k)^2)\cos^2(2\theta)},$$

$$X = 2c_1\xi_k + 2c_2\delta\cos^2(2\theta),$$

$$Y = \frac{2c_2\left(2c_1^2k^4\delta + \alpha\Delta^2\mu - c_1k^2(2\alpha\Delta^2 + 3\delta\mu) + \delta(\beta^2 + \mu^2)\right)}{\sqrt{\beta^2\Delta^2 + (\beta^2\delta^2 + (\alpha\Delta^2 - \delta\xi_k)^2)\cos^2(2\theta)}},$$

$$Z = \left(-\delta^2 - \alpha^2\Delta^2 + \frac{\beta^2\delta^2 + (\alpha\Delta^2 - \beta\xi_k)^2}{\sqrt{\beta^2\Delta^2 + (\beta^2\delta^2 + (\alpha\Delta^2 - \delta\xi_k)^2)\cos^2(2\theta)}}\right). \quad (24)$$

Here we introduced $c_1 = \frac{1}{4}\left(\frac{1}{m_1} + \frac{1}{m_2}\right)$ and $c_2 = \frac{1}{4}\left(\frac{1}{m_1} - \frac{1}{m_2}\right)$.

For brevity, we focus on the case when ellipticity is strong enough ($\delta > \alpha\Delta$, see Sec. III A) and consider the winding numbers for the two nodal points, which emerge at $\beta = \Delta$ along the diagonals, and then move merge with the existing nodal points at $\beta = \beta_{crit} > \Delta$.

Because of C_4 rotational symmetry, we again focus on the nodal points at $0 < \theta < \pi/4$. We computed the determinant of (22) numerically for $\Delta = 1, \beta = 1.002, \mu = 10, \alpha = -1.5, m_2/m_1 = 2$, and verified that the winding numbers for the new nodal point, which appears at $\beta = \Delta$, and the "old" nodal point, with which the new one eventually merges, have opposite signs of the winding number.

We next discuss the computation of the winding numbers in the "geometrical" approach, when we transform different nodal points into the same location. For $\beta \geq \Delta$, the two emerging nodal points are still close to the diagonals, and we can expand E_k^- in powers of ξ and $\cos 2\theta$. The expansion yields

$$(E_k^-)^2 \approx E_{\rm lin}^2 = \xi^2 + F(\theta), \quad (25)$$

where ξ is a function of β from Eq. (14) (one should choose the solution for which $\xi = 0$ for $\beta = \Delta$), and

$$F(\theta) = \cos^2(2\theta)\left[\delta^2 + \Delta^2\alpha^2 - \frac{(\Delta^2\alpha - \xi\delta)^2 + |\beta|^2\delta^2}{|\beta|\Delta}\right] \\ + \cos^4(2\theta)\frac{\left[(\Delta^2\alpha - \xi\delta)^2 + |\beta|^2\delta^2\right]^2}{4|\beta|^3\Delta^3} + (\Delta - |\beta|)^2. \quad (26)$$

We plot $E_{\rm lin}^2$ as a function of θ in Fig. 4. The new nodal points emerge at $\beta = \Delta$, at $\xi = F = 0$. As β increases, the two nodal points split and move towards already existing nodal points.
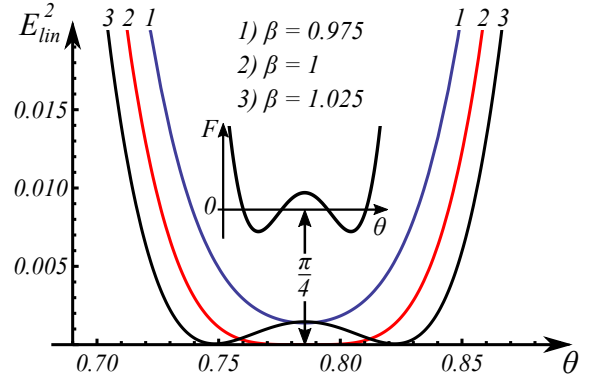

FIG. 4. Angular dependence of $E_{\rm lin}^2$, Eq. (25), for three values of β, smaller, equal, and larger than Δ, which we set equal to one in proper units. Inset: $F(\theta)$ as a function of the angle θ for $\beta = 1.025 > \Delta$. The minima of F correspond to the locations of emerging nodal points. We set $\mu = 10, \alpha = -1.5, m_2/m_1 = 2$.

To calculate the winding numbers of these nodal points we transform to the (ξ, F) plane, where the two nodal points

are moved to the same ξ and F. In distinction to the case of circular pockets, the nodal points are now located at finite ξ and F, given by $E_{\text{lin}} = 0$. Still, the integration contour C is the same for both nodal points, and one can extract the winding numbers from the bypass directions. Consider the nodal point in the upper panel of Fig. 5. Let us choose the counterclockwise bypass along the closed contour in the (k_x, k_y)-plane. In (ξ, F) plane, this bypass starts at $\xi = 0$, $F(\theta) > 0$, proceeds to the point $\xi < 0$, $F(\theta) = 0$ and then reaches $\xi = 0$, $F(\theta) < 0$. This is clockwise bypass in the (ξ, F)-plane. For the nodal point in the lower panel of Fig. 5, the same consideration shows that the bypass direction in the (ξ, F)-plane changes to counterclockwise. This implies that the winding numbers for the two emerging nodal points are opposite.

The winding numbers of the original nodal points can be obtained in the same way as was done for circular pockets because these nodal points survive when the ellipticity parameter δ vanishes. Comparing the directions of bypass in Figs. 3 and 5 we see that the nodal points, which eventually merge and disappear, always have the winding numbers of opposite sign.
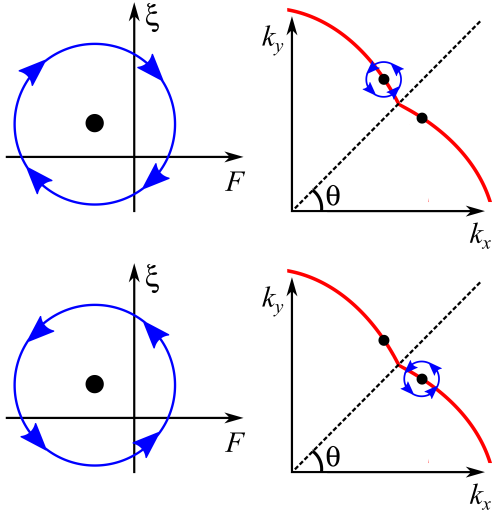

FIG. 5. The case of elliptical pockets. Bypass trajectories around the emerging nodal points (black dots) at $\beta > \Delta$ for two sets of co-ordinates: (k_x, k_y) in the right panel and (ξ, F) in the left panel (see the text for the definitions of ξ and F). In left panel, the two nodal points are mapped into the same point in the new coordinates. Opposite signs of the winding numbers for these two points are due to different directions of bypass, as shown in the left panel.

C. Numerical analysis

1. The numerical procedure

We supplement our analytical calculations with the numerical analysis. We use the computational procedure introduced in Ref. [32]. It uses discrete grid functions for Berry connection and Berry curvature. In order to calculate these functions, one has to define the wave function of the system. In Nambu notation, a field operator is $\Psi = (v_k^c c_k^\dagger + u_k^c c_{-k} + v_k^d d_k^\dagger + u_k^d d_{-k})$, where $u_k^c, v_k^c, u_k^d, v_k^d$ are Bogoliubov transformation coefficients. The wave function of the system $|n(\mathbf{k})\rangle$ is then a 4-component vector [34] made out of Bogoliubov coefficients. We need the two wave functions which correspond to eigenvalues $\pm E^-(k)$, which, we remind, describe the excitation branch with the nodes.

For the numerical computation of the Berry curvature, we follow Ref. [32] and introduce the grid on the BZ, i.e., coarse-grain momenta to $\vec{k} = k_{ij} = \left(2\pi i/a_x, 2\pi j/a_y\right)$, where a_x, a_y are grid spacings, each a fraction of the interatomic spacing. It was argued that the value of B doesn't depend on grid spacing as long as each elementary cell contains no more than one nodal point. We next introduce a link variable $\tilde{A}_{\vec{\delta}}(\vec{k})$ on a grid (a "discrete Berry connection"):

$$\tilde{A}_{\vec{\delta}}(\vec{k}) = \langle n(\vec{k})|n(\vec{k} + \vec{\delta})\rangle/N. \qquad (27)$$

where $N = |\langle n(\vec{k})|n(\vec{k} + \vec{\delta})\rangle|$ – is the normalization factor, and $\delta_x = (2\pi/a_x, 0)$, $\delta_y = (0, 2\pi/a_y)$. This $\tilde{A}_{\vec{\delta}}(\vec{k})$ determines the phase, which $\left|n(\vec{k})\right\rangle$ acquires under the change from $\vec{k}$ to $\vec{k}+\vec{\delta}$. The total phase change over an elementary closed loop adjacent to a particular $\vec{k} = k_{ij}$ (i.e., a particular combination of i, j) is

$$K(\vec{k}) = \tilde{A}(\vec{k})_{\vec{\delta}_x} \tilde{A}(\vec{k} + \vec{\delta}_x)_{\vec{\delta}_y} \tilde{A}(\vec{k} + \vec{\delta}_y)_{\vec{\delta}_x}^{-1} \tilde{A}(\vec{k})_{\vec{\delta}_y}^{-1}. \qquad (28)$$

Taking the logarithm of K we obtain the phase change over a loop:

$$\tilde{B}(\vec{k}) = \frac{1}{i}\ln K(\vec{k}) = \phi(\vec{k}). \qquad (29)$$

If there is no node inside a loop for a given $\vec{k} = \vec{k}_0$, the overall phase change is zero. If a given loop encircles a nodal point, then, within the loop, one moves from the lower to the upper branch of the Dirac spectrum (or vise versa), and the phase changes by $\pm 2\pi$. Accordingly, $\tilde{B}(\vec{k}_0)/2\pi$ gives the winding number of this nodal point. In the ideal situation, $\tilde{B}(\vec{k})$ will be non-zero only for a discrete set of $\vec{k}_0$, equal to the number of nodal points. In numerical calculations, however, the logarithm in Eq. (29) often strongly oscillates between 2π and -2π, if a nodal point is near the trajectory along the loop. To avoid this complication, we add to the

Hamiltonian the term $m\sigma^y$ and compute $\tilde{B}(\vec{k})$ for all $\vec{k}$ in the BZ. This term makes the value of the logarithm well defined, but at the same time, it couples lower and upper branches of the Dirac spectrum, and, as a result, $\tilde{B}(\vec{k})$ becomes non-zero for all **k** in the BZ. Still, as long as m is small, the numerics clearly shows an enhancement of the magnitude of $\tilde{B}$ near a node. Because our primary goal is to check the signs of the winding numbers, it is sufficient to compute $\tilde{B}(\vec{k})$ for a small but finite m and check the sign of $\tilde{B}(\vec{k})$ near each nodal point.

2. Circular pockets

The results of our calculations of $\tilde{B}(\vec{k})$ for circular pockets are shown in Fig. 6. We found that eight nodal points have the winding numbers ± 1. This is fully consistent with the analytical result. We also see from Fig. 6 that there is a checkerboard order of nodal points with positive and negative values of the winding number. This is again consistent with the analytical results.
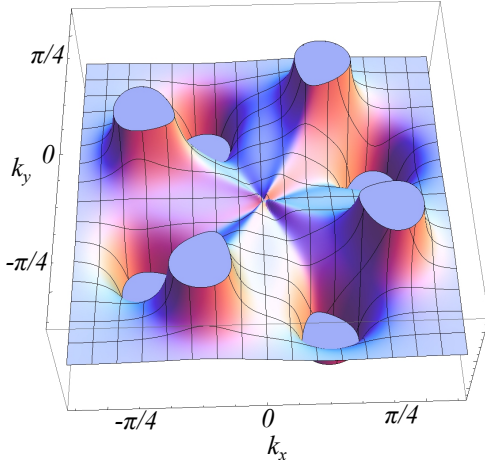
FIG. 6. The grid Berry curvature $\tilde{B}$ for the case of circular electron pockets. We used $\beta = 0.5, \mu = 1, \Delta = 1, \alpha = 1.5$. The grid shows the checkerboard order of positive and negative winding numbers for the eight nodal points.

3. Elliptical pockets

For elliptical pockets, we used as the point of departure the effective band Hamiltonian representing the low-energy band E^-, which has nodal points. We introduce a 2×2 matrix Hamiltonian, which gives the dispersion in Eq. (13) and apply the numerical procedure, described above. We plot the Berry curvature as a function of $|\vec{k}|$ and θ in Fig. 7. As we can see from this figure, in the region around the nodal
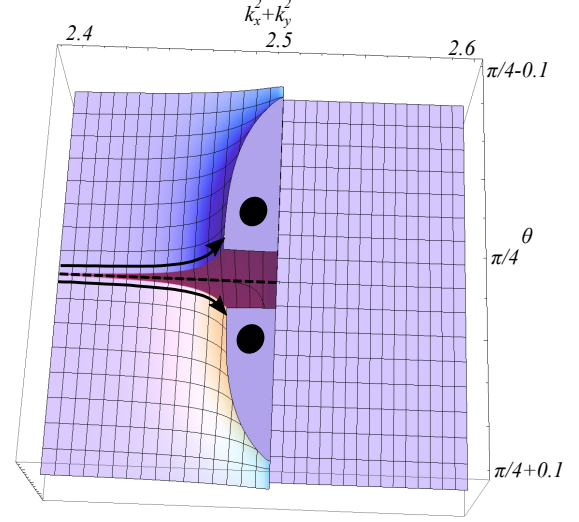
FIG. 7. The grid Berry curvature $\tilde{B}$ for the two emerging nodal points in the case when the electron pockets are elliptical. The positions of the nodal points are shown by black dots. Unusual shape of the plateaus around nodal points is caused by the choice of polar coordinates. The arrows show where the grid Berry curvature is positive, and where it is negative. We used $\mu = 10, \alpha = -1.5, \beta = 1.01, \Delta = 1, m_2/m_1 = 2$.

points, the Berry curvature saturates at a positive value near one point and at negative value near the other. This leads to opposite signs of the winding numbers around these points. This is again fully consistent with the analytical results.

IV. A TWO-BAND d-WAVE SUPERCONDUCTOR
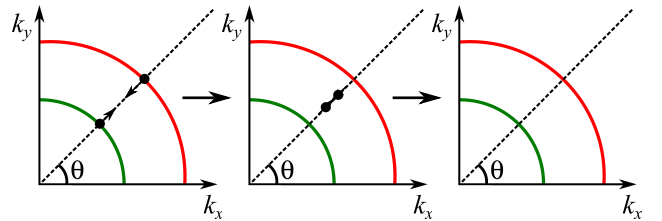
A. The model

FIG. 8. The nodal points (black dots) in a d-wave FeSC with FSs made out of d_{xz} and d_{yz} orbitals. Red and green lines are the two FSs from the normal state. When the magnitude of the d-wave gap Δ increases, nodal points move along the BZ diagonal, and merge and disappear at some Δ_{crit}.

We next consider the model of FeSC with the d-wave gap structure [19, 23]. The model is for a heavily hole doped FeSC with two $\Gamma-$ centered hole pockets and no elec-

tron pockets. The hole pockets are made out of d_{xz} and d_{yz} orbitals, and orbital content is rotated by 90° between the two pockets. Because the orbital content varies along the Fermi surfaces, the interactions in the band basis are angle-dependent and have both s-wave and d-wave components. We assume that d-wave interaction is attractive and stronger than s-wave one, such that the system develops $d_{x^2-y^2}$ superconductivity below a certain T.

The d-wave gap equation in the band basis has been analyzed in [19, 23]. The kinetic energy is

$$H_0 = \sum_{k,\alpha} \left(\epsilon_{1,k} c_{1,k}^\dagger c_{1,k} + \epsilon_{2,k} c_{2,k}^\dagger c_{2,k} \right), \tag{30}$$

where $\epsilon_{1,2,k} = \mu - k^2/(2m_{1,2})$ and we consider $m_1 \neq m_2$. By symmetry, the pairing interaction couples intra-pocket pairing condensates $\langle c_{1,k\alpha}^\dagger c_{1,-k\beta}^\dagger \rangle$ and $\langle c_{2,k\alpha}^\dagger c_{2,-k\beta}^\dagger \rangle$, and inter-pocket pairing condensates $\langle c_{1,k\alpha}^\dagger c_{2,-k\beta}^\dagger \rangle$ and $\langle c_{2,k\alpha}^\dagger c_{1,-k\beta}^\dagger \rangle$. For the case when the interaction in the band basis is obtained from a local Hubbard-Hund interaction in the orbital basis, the anomalous part of the BCS Hamiltonian is

$$H_\Delta = \Delta_a \sum_k i\sigma_{\alpha\beta}^y \left(c_{1,k\alpha}^\dagger c_{1,-k\beta}^\dagger - c_{2,k\alpha}^\dagger c_{2,-k\beta}^\dagger \right) + \\ + \Delta_b \sum_k i\sigma_{\alpha\beta}^y \left(c_{1,k\alpha}^\dagger c_{2,-k\beta}^\dagger + c_{2,k\alpha}^\dagger c_{1,-k\beta}^\dagger \right) + \text{H.c.} \tag{31}$$

where $\Delta_a = \Delta\cos2\theta$ and $\Delta_b = \Delta\sin2\theta$.

Diagonalizing this BCS Hamiltonian, we obtain two bands, a and b, with the dispersion

$$E_{a,b}(k) = \sqrt{\Delta^2\cos^2(2\theta) + \epsilon_{a,b}^2(k)}, \tag{32}$$

where

$$\epsilon_{a,b}(k) = \text{sgn}(\epsilon_{1,k}+\epsilon_{2,k})\sqrt{\left(\frac{\epsilon_{1,k}+\epsilon_{2,k}}{2}\right)^2 + \Delta^2\sin^2(2\theta)} \pm \frac{\epsilon_{1,k}-\epsilon_{2,k}}{2} \tag{33}$$

When the two Fermi surfaces are far apart, $\epsilon_a \approx \epsilon_{1,k}$ and $\epsilon_b \approx \epsilon_{2,k}$. In this limit, we have a conventional d-wave gap structure with nodal points on each Fermi surface, along the diagonals. However, when Δ is comparable to the energy difference between ϵ_1 and ϵ_2, when one of ϵ vanishes, the nodal points move away from the two Fermi surfaces into the region between them (see Fig. 8). At some critical Δ, the two nodal points along each diagonal merge and disappear, leaving a d-wave superconductor nodeless.

B. The winding number

Without loss of generality we set $m_2 > m_1$. Inside the smaller Fermi surface $\epsilon_{1,k} < 0$ and $\epsilon_{2,k} < 0$. Upon crossing the smaller Fermi surface $\epsilon_{1,k}$ changes sign, but $\epsilon_{2,k}$ remains negative, i.e., $\text{sgn}(\epsilon_{1,k} + \epsilon_{2,k}) = -1$. Near the larger Fermi
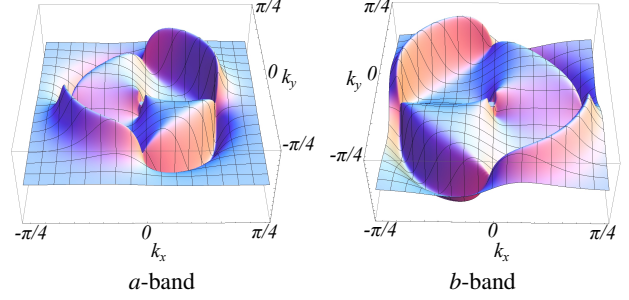

FIG. 9. The grid Berry curvature $\tilde{B}$ computed for the two bands a and b (each with nodal points) for a model of a d-wave superconductor, Eq. (32). We set $\Delta = 0.3, \mu = 1, \alpha = 1$. We see that the sign of the Berry curvature changes between the two nodal points along the same diagonal.

surface $\epsilon_{2,k} \simeq 0$ and $\epsilon_{1,k} > 0$. Then $\text{sgn}(\epsilon_{1,k} + \epsilon_{2,k}) = 1$. As a result, near each of the two nodal points $\epsilon_a = \xi = -\epsilon_b$. Using this, we construct effective Dirac Hamiltonians H_a and H_b:

$$H_{a,b} = \begin{pmatrix} \pm\xi & 2\Delta(\theta - \pi/4) \\ 2\Delta(\theta - \pi/4) & \mp\xi \end{pmatrix}. \tag{34}$$

The corresponding matrices A are

$$A_{a,b} = \begin{pmatrix} 2\Delta & 0 \\ 0 & \pm\frac{d\xi}{dk} \end{pmatrix} \tag{35}$$

Then $sign[\det(A_a)] = -sign[\det(A_b)]$, i.e., the two nodal points along each diagonal have opposite winding numbers.

C. Numerical analysis

We computed the Berry curvature separately for the effective Hamiltonians H_a and H_b. The results are shown in Fig. 9. We see that the Berry curvature has opposite signs for a pair of nodal points along the same diagonal, hence these points have the winding numbers of opposite sign. This agrees with the analytic result.

V. CONCLUSIONS

In this paper we analyzed the merging and disappearance of the nodal points in FeSCs from topological perspective. We considered two models with different pairing symmetry – s-wave ($s^\pm$) and d-wave. For an s^{+-}-wave superconductor we considered the model with accidental nodes on the two electron pockets. We manipulated the position of the nodes by varying the degree of hybridization between the two electron pockets. We considered first the special case when the electron pockets are circular, and then a generic case when they are elliptical. In both cases increasing the

strength of hybridization gives rise to the Lifshitz transition in which neighboring nodal points merge and annihilate. For the case of circular pockets we showed that of eight nodal points four have positive winding number $Q = +1$ and four have $Q = -1$. We showed that the nodal points, which merge at the Lifshitz transition, have opposite winding numbers. In the case of elliptical pockets, we focused on the case when, upon the increase of hybridization, first eight new nodal points are created in pairs, and then new nodal points merge with the existing ones. We showed that in each pair the two emerging nodes have opposite signs of the winding number. And the winding numbers of the newly created and the existing nodal points, which merge and annihilate at larger hybridization, are also opposite. As a result, the net topological invariant is conserved in the Lifshitz transition and from this perspective the transition from a nodal to full gap s^{+-} superconductor can be labeled as non-topological one.

For d-wave gap symmetry we considered a model with two hole pockets made out of d_{xz} and d_{yz} orbitals. The pairing condensate in this model necessary contains intra-pocket and inter-pocket components. The latter move the nodal points away from the Fermi surfaces, into the area in between the pockets. As the pairing gap increases (or the distance between the pockets decreases), the two nodal points along each diagonal come closer to each other and eventually merge and disappear via Lifshitz transition. We showed that the winding numbers of these nodal points are again $Q = \pm 1$. Then the net winding number is zero, and the Lifshitz transition in a d-wave case also can be labeled as non-topological.

The merging and annihilation of nodal points has been well studied in Dirac and Weyl semi-metals which undergo a transition into an insulator under a variation of certain system parameters [24]. Several authors have shown that in a semi-metal-to-insulator transition, the merging nodal points have opposite winding numbers [25, 26]. We demonstrated that the same is true in nodal-to-full gap transitions in s-wave and d-wave FeSCs.

Appendix A: Gap opening

In the Section III C 1 we make some remarks about the numerical calculation of the winding numbers in a superconductor. As we said in the main text, to regularize the numerical procedure, it is convenient to add a small mass term $m\sigma^y$ to the dispersion. Such a term opens up the gap in the excitation spectrum allowing one to define unambiguously the sign of the logarithm in Eq. (29). However, numerical analysis shows that this term gives rise to non-zero value of the logarithm for a loop which does not enclose nodal points. Here we show analytically that this is indeed the case.

To be brief, consider a simple 2×2 BdG Hamiltonian with the additional $m\sigma^y$ term:

$$H = \begin{pmatrix} \xi - a & \Delta - b - im \\ \Delta - b + im & -\xi + a \end{pmatrix}. \qquad (A1)$$

For $m = 0$, this Hamiltonian has the nodal point at $\xi = a, \Delta = b$. For a non-zero m, we introduce link variable, according to Eq. (27), and obtain $\tilde{A}(\xi, \Delta)_{\vec{d\xi}}$ in the form

$$\tilde{A}(\xi, \Delta)_{\vec{d\xi}} = \frac{X_1 + (\xi - a)d\xi - (\xi + d\xi + a)\sqrt{X_1} + \sqrt{X_2}\left((a - \xi)\sqrt{X_1}\right)}{2\mathcal{N}\sqrt{\left(X_1 + (a - \xi)\sqrt{X_1}\right)\left(X_2 + (a - \xi - d\xi)\sqrt{X_2}\right)}},$$

$$X_1 = m^2 + (b - \Delta)^2 + (a - \xi)^2,$$

$$X_2 = m^2 + (b - \Delta)^2 + (a - \xi - d\xi)^2,$$

$$(A2)$$

where $\mathcal{N}$ - is the normalization factor. Let us start from the origin of the (ξ, Δ)-plane and select the loop such that it does not encounter the nodal point. For this we choose $d\xi < a, d\Delta < b$, where $d\xi, d\Delta$ are the elementary steps (these are equivalent to δ_x, δ_y in the main text). We have

$$K(\xi, \Delta) = \tilde{A}(0, 0)_{\vec{d\xi}} \tilde{A}(d\xi, 0)_{\vec{d\Delta}} \tilde{A}(0, d\Delta)_{\vec{d\xi}}^{-1} \tilde{A}(0, 0)_{\vec{d\Delta}}^{-1}. \quad (A3)$$

To first order in $d\xi$ and $d\Delta$

$$K = 1 + \frac{im\left(2a^2 + b^2 + m^2 + 2a\sqrt{a^2 + b^2 + m^2}\right)d\xi d\Delta}{2\sqrt{a^2 + b^2 + m^2}\left(a^2 + b^2 + m^2 + a\sqrt{a^2 + b^2 + m^2}\right)^2}. \qquad (A4)$$

It is obvious from this expression that for any finite m, $\ln K \neq 0$.

[1] D. J. Thouless, M. Kohmoto, M. P. Nightingale, and M. den Nijs, Phys. Rev. Lett. **49**, 405 (1982).

[2] B. Simon, Phys. Rev. Lett. **51**, 2167 (1983).

[3] M. Berry, Proceedings of the Royal Society of London A: Mathematical, Physical and Engineering Sciences **392**, 45 (1984),

http://rspa.royalsocietypublishing.org/content/392/1802/45.full.pdf.

[4] B. A. Bernevig and S.-C. Zhang, Phys. Rev. Lett. **96**, 106802 (2006).

[5] B. A. Bernevig, T. L. Hughes, and S.-C. Zhang, Science **314**, 1757 (2006), http://science.sciencemag.org/content/314/5806/1757.full.pdf.

[6] X. Wan, A. M. Turner, A. Vishwanath, and S. Y. Savrasov, Phys. Rev. B **83**, 205101 (2011).

[7] S.-Y. Xu, I. Belopolski, N. Alidoust, M. Neupane, G. Bian, C. Zhang, R. Sankar, G. Chang, Z. Yuan, C.-C. Lee, S.-M. Huang, H. Zheng, J. Ma, D. S. Sanchez, B. Wang, A. Bansil, F. Chou, P. P. Shibayev, H. Lin, S. Jia, and M. Z. Hasan, Science **349**, 613 (2015), http://science.sciencemag.org/content/349/6248/613.full.pdf.

[8] J. G. Bednorz and K. A. Müller, Zeitschrift für Physik B Condensed Matter **64**, 189 (1986).

[9] C. C. Tsuei and J. R. Kirtley, Rev. Mod. Phys. **72**, 969 (2000).

[10] D. J. Scalapino, Rev. Mod. Phys. **84**, 1383 (2012).

[11] Y. Kamihara, T. Watanabe, M. Hirano, and H. Hosono, Journal of the American Chemical Society **130**, 3296 (2008), pMID: 18293989, http://dx.doi.org/10.1021/ja800073m.

[12] C. de la Cruz, Q. Huang, J. Lynn, J. Li, W. R. II, J. Zarestky, H. Mook, G. Chen, J. Luo, N. Wang, *et al.*, Nature **453**, 899 (2008).

[13] C. Liu, T. Kondo, R. M. Fernandes, A. D. Palczewski, E. D. Mun, N. Ni, A. N. Thaler, A. Bostwick, E. Rotenberg, J. Schmalian, *et al.*, Nature Physics **6**, 419 (2010).

[14] M. Putti, I. Pallecchi, E. Bellingeri, M. Cimberle, M. Tropeano, C. Ferdeghini, A. Palenzona, C. Tarantini, A. Yamamoto, J. Jiang, *et al.*, Superconductor Science and Technology **23**, 034003 (2010).

[15] T. Hanaguri, S. Niitaka, K. Kuroki, and H. Takagi, Science **328**, 474 (2010), http://science.sciencemag.org/content/328/5977/474.full.pdf.

[16] T. A. Maier, S. Graser, P. J. Hirschfeld, and D. J. Scalapino, Phys. Rev. B **83**, 100515 (2011).

[17] P. Hirschfeld, M. Korshunov, and I. Mazin, Reports on Progress in Physics **74**, 124508 (2011).

[18] M. Khodas and A. V. Chubukov, Phys. Rev. Lett. **108**, 247003 (2012).

[19] A. V. Chubukov, O. Vafek, and R. M. Fernandes, Phys. Rev. B **94**, 174518 (2016).

[20] I. M. Lifshitz, Sov. Phys. JETP **11**, 1130 (1960).

[21] C. Liu, A. D. Palczewski, R. S. Dhaka, T. Kondo, R. M. Fernandes, E. D. Mun, H. Hodovanets, A. N. Thaler, J. Schmalian, S. L. Bud'ko, P. C. Canfield, and A. Kaminski, Phys. Rev. B **84**, 020509 (2011).

[22] A. Hinojosa and A. V. Chubukov, Phys. Rev. B **91**, 224502 (2015).

[23] E. M. Nica, R. Yu, and Q. Si, npj Quantum Materials **2**, 24 (2017).

[24] O. Vafek and A. Vishwanath, Annual Review of Condensed Matter Physics **5**, 83 (2014), https://doi.org/10.1146/annurev-conmatphys-031113-133841.

[25] S. Murakami and S.-i. Kuga, Phys. Rev. B **78**, 165313 (2008).

[26] S. Murakami, New Journal of Physics **9**, 356 (2007).

[27] M. Z. Hasan and C. L. Kane, Rev. Mod. Phys. **82**, 3045 (2010).

[28] X.-L. Qi and S.-C. Zhang, Rev. Mod. Phys. **83**, 1057 (2011).

[29] B. A. Bernevig and T. L. Hughes, *Topological insulators and topological superconductors* (Princeton University Press, 2013).

[30] E. Fradkin, *Field theories of condensed matter physics* (Cambridge University Press, 2013).

[31] M. Sato and Y. Ando, Reports on Progress in Physics **80**, 076501 (2017).

[32] T. Fukui, Y. Hatsugai, and H. Suzuki, Journal of the Physical Society of Japan **74**, 1674 (2005), arXiv:0503172 [cond-mat].

[33] A. B. Vorontsov, M. G. Vavilov, and A. V. Chubukov, Phys. Rev. B **81**, 174538 (2010).

[34] P. Heinzner, A. Huckleberry, and M. Zirnbauer, Communications in Mathematical Physics **257**, 725 (2005).